学位論文

Quantification of Vascular Function in Coronary and Brachial Arteries

（冠動脈および上腕動脈の血管機能の定量評価）

2016 年 3 月

北海道大学

富山　勇輝

Yuuki Tomiyama

学位論文

Quantification of Vascular Function in Coronary and Brachial Arteries

（冠動脈および上腕動脈の血管機能の定量評価）

2016 年 3 月

北海道大学

富山　勇輝

Yuuki Tomiyam

目　次

発表論文目録および学会発表目録 - 1 -

Introductions - 2 -

Chapter 1
Quantification of Myocardial Blood Flow with Dynamic Perfusion MRI - 3 -
Introduction - 3 -
Material and Methods - 4 -
Results - 10 -
Discussion - 19 -
Conclusion - 22 -

Chapter 2
Quantitative Measurements of Brachial Artery Vascular Function Using Automated　Oscillometric Methods Comparison with Ultrasound - 23 -
Introduction - 23 -
Material and Methods - 24 -
Results - 31 -
Discussion - 36 -
Conclusion - 40 -

Conclusions - 41 -

謝辞 - 42 -

参考文献 - 43 -

発表論文目録および学会発表目録

本研究の一部は以下の論文に発表した。

1. Yuuki Tomiyama, Osamu Manabe, Noriko Oyama-Manabe, Masanao Naya, Hiroyuki Sugimori, Kenji Hirata, Yuki Mori, Hiroyuki Tsutsui, Kohsuke Kudo, Nagara Tamaki, Chietsugu Katoh: Quantification of myocardial blood flow with dynamic perfusion 3.0 Tesla MRI: Validation with (15) O-water PET. Journal of Magnetic Resonance Imaging, 2015 Sep;42(3): 754-62.

2. Yuuki Tomiyama, Keiichiro Yoshinaga, Satoshi Fujii, Noriki Ochi, Mamiko Inoue, Mutsumi Nishida, Kumi Aziki, Tatsunori Norie, Chietsugu Katoh, Nagara Tamaki:Accurate quantitative measurements of brachial artery cross-sectional vascular area and vascular volume elastic modulus using automated oscillometric measurements: comparison with brachial artery ultrasound.Hypertension Research, 2015 Jul; 38(7): 478-84.

本研究の一部は以下の学会に発表した。

1. Yuuki Tomiyama, Chietsugu Katoh, Osamu Manabe, Noriko Oyama-Manabe, Keiichiro Yoshinaga, Nagara Tamaki, Quantification of Myocardial Blood Flow with 3.0 Tesla MRI perfusion image in healthy persons: Comparison with 15O-H2O PET, 59th Society of Nuclear Medicine, Maiami, Florida 2012.6.12

2. 富山勇輝、吉永恵一郎、越智典樹、井上真美子、井上真美子、西田睦、西尾沙織、藤井聡、玉木長良、オシロメトリック法による自動血管機能測定装置を用いた新たな血管反応性検出法、第 36 回日本高血圧学会　大阪、2013.10.26

3. 富山勇輝、真鍋治、真鍋徳子、菊池穏香、杉森博行、加藤千恵次、玉木長良、酸素 15 標識水 PET を用いた 3.0T MRI 心臓 perfusion による 心筋血流定量法の開発：局所解析への応用、第 70 回　日本放射線技術学会　横浜、2014.4.10

4. 富山勇輝、真鍋治、真鍋徳子、納谷昌直、菊池穏香、加藤千恵次、玉木長良、Quantification of Myocardial Blood Flow with Perfusion MRI using Validation with 15O-H2O PET ： Application to Regional Analysis、第 54 回　日本核医学会総会　大阪、2014.11.8

Introductions

Quantification of vascular function has been to be useful method for evaluation of the prognosis of cardiovascular events. Especially, dysfunction of the coronary or brachial artery has reported to be strongly associated with cardiovascular events.

In order to assess the coronary artery function, positron emission tomography (PET) is widely used, which enables to evaluate the clinical information, such as myocardial blood flow (MBF).

Representative Case of ^{15}O-H_2O PET

Polar map of the patient
with LAD stenosis t rest and stress

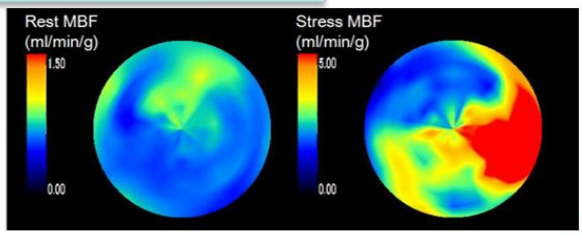

Evaluation of peripheral artery is also important for detecting earliest stage of atherosclerosis. Ultrasound imaging of the brachial artery is considered to be the standard measurement and used to obtain the information of vascular function.

Measurement of brachial artery ultrasound

Brachial artery ultrasound
enables to measure diameter and
flow-mediated dilatation (%FMD)

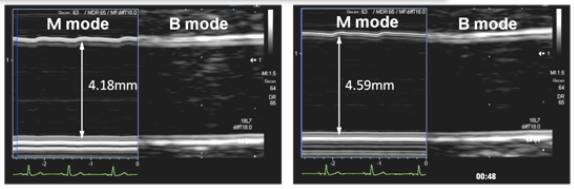

Rest After cuff stress

However, these measurements are clinically limited.PET study needs a cyclotron equipment, brachial artery ultrasound required experienced operator. Therefore, alternative simplified method should be developed.

Recently, we published two kinds of new methods to quantify the vascular function. One is MBF quantification method using magnetic resonance imaging (MRI), and the other is automated oscillometric method to measure the diameter and elasticity of the brachial artery.

In the first study, we compared MBF quantified from MRI with PET, which yields standard MBF. In the second study, we compared the diameter and elasticity of the brachial artery estimated from the automated oscillometric measurement with the ultrasound imaging.

Chapter 1

Quantification of Myocardial Blood Flow with Dynamic Perfusion MRI

Yuuki Tomiyama, Osamu Manabe, Noriko Oyama-Manabe, Masanao Naya, Hiroyuki Sugimori, Kenji Hirata, Yuki Mori, Hiroyuki Tsutsui, Kohsuke Kudo, Nagara Tamaki and Chietsugu Katoh

Introduction

Myocardial blood flow (MBF), coronary flow reserve (CFR), and the morphological extent of coronary stenosis do not provide the same information and are not inversely correlated[1, 2]. The quantification of MBF and CFR is a useful method for evaluating functional severity, even in patients with balanced multivessel diseases and microcirculatory disturbances[3-6]. We previously validated the usefulness of the single-tissue compartment model for quantifying MBF and CFR on the basis of positron emission tomography (PET)[7] and multidetector row computed tomography (MDCT) images [8]. Our model used the K1 value as the uptake rate for contrast media from the left ventricular (LV) chamber into the LV myocardium and the k2 value as the outflow rate for contrast media from the LV myocardium into the LV chamber.

Magnetic resonance imaging (MRI) is in widespread clinical use and is employed for cardiac examinations. Stress MR perfusion provides information about the functional severity of coronary artery stenosis[9]. In particular, 3.0 Tesla (3T) MRI has a high spatial resolution power that allows the more precise evaluation of coronary artery disease (CAD). Cheng et al. reported that perfusion MRI at 3T was superior to that at 1.5T with visual assessment for the prediction of CAD[10]. Furthermore, MRI has the potential to estimate MBF from time–intensity curves (TICs) for the LV tissue and LV cavity using extraction fraction models. Indeed, several studies have used 1.5T MRI to quantify MBF values, which were validated by comparing those obtained from conventional PET[11-14]. A prior MR perfusion study using the Patlak plot method employed only the K1 value and

ignored the k2 value[15].

The present study aimed to quantify MBF and CFR using dynamic perfusion MRI at 3T and compare the findings with those of ^{15}O-water PET as the gold standard in healthy subjects. The results were also compared between the healthy subjects and CAD patients. The second aim was to compare the effectiveness of our single-tissue compartment model[7, 8] and the well-known Patlak plot method[15].

Material and Methods

Study Subjects

This prospective study was approved by the local Ethics Committee. Twenty healthy male volunteers (age, 28.4 ± 8.9 years) with no history of cardiovascular disease were enrolled (Table 1). Written informed consent was obtained from each subject.

Ten patients (6 males; age, 67.2 ± 7.8 years) with angiographically confirmed CAD (>75% coronary artery stenosis) who underwent MRI were also included.

Study Protocol

Each subject underwent both MRI and ^{15}O-water PET under adenosine triphosphate (ATP) infusion (160 μg/kg/min) and at rest. The MRI and ^{15}O-water PET examinations were conducted in random order. All subjects refrained from consuming caffeine-containing beverages for at least 24 h and from smoking for at least 4 h before the examinations, as previously recommended[16, 17].

Using the first 10 subjects as a pilot group, we estimated the extraction fraction from the inflow rate of Gd-DTPA ($K1_{MRI}$) and MBF using ^{15}O-water PET (MBF_{PET}) with the Renkin–Crone model[7]. We validated the findings by comparing them with MBF calculated from $K1_{MRI}$ (MBF_{MRI}) using the estimated extraction fraction for the remaining 10 subjects (validation group). The CFRs for MRI and PET were also compared. The interobserver variability in MBF_{MRI} was assessed by two independent observers. MBF_{MRI} and CFR_{MRI} values were also obtained for the CAD patients.

^{15}O-water PET Protocol

After obtaining a transmission scan, we acquired dynamic ^{15}O-water PET scans using the HR+ PET scanner (Siemens, Erlangen, Germany)[16]. All emissions and transmissions were acquired in the two-dimensional mode and reconstructed using filtered back

projection with a Hanning filter (cutoff, 0.4). A 5-min transmission scan was acquired for the attenuation correction of all subsequent emission scans. Then, ^{15}O-water (1,500 MBq) was gradually infused (100 s) into the antecubital vein and a 20-frame dynamic PET scan comprising 6 × 5-s, 6 × 15-s, and 8 × 30-s frames was acquired over 6 min.

^{15}O-water PET Image Analysis

PET images were reconstructed using vendor-supplied filtered back-projection software (ECAT v7.2) with a 10-mm Hann window for the ramp filter. The frames included 63 transaxial slices (128 × 128 voxels, 3.4 × 3.4 × 2.4 mm). We calculated MBF (mL/min/g) from regions of interest (ROIs) plotted in the LV chamber and myocardium using in-house software and a previously described single-tissue compartment model[7, 18] CFR was computed as the ratio of the MBF during ATP stress to MBF at rest[19].

MRI Protocol

Cardiac MRI was performed using a 3T whole-body scanner (Achieva Tx; Philips Medical Systems, Best, The Netherlands) with a 32-channel phased-array receiver torso-cardiac coil. A fully flexible dual-source RF transmission system for patient-adaptive local radiofrequency shimming was used. This achieves optimal B1 homogeneity, even with a moving heart[20].

MRI Phantom

For the accurate quantification of MBF using myocardial first-pass perfusion, a proportional relationship is required between the signal intensity and the concentration of the gadolinium contrast medium[21]. Therefore, we conducted a phantom study for the preliminary estimation of the relationship. The blood was immediately heparinized using a small amount of heparin to avoid blood coagulation, and the sample was continuously mixed and maintained at room temperature until just before image acquisition. To determine the relationship between the MR blood signal intensity and the Gd-DTPA concentration, MR images of eight tubes (4 × 3 × 2 cm each) containing blood samples with different concentrations of Gd-DTPA (0, 0.10, 0.25, 0.50, 0.75, 1.0, 1.5, and 2.0 mmol/L; 14 mL of blood and 1 mL of blood or diluted Gd-DTPA) were placed at the same distance from the torso-cardiac coil as that from the heart in a human body.MRI was performed using the turbo field-echo technique with saturation recovery (SR) magnetization preparation under the following conditions: repetition time/echo time

(TR/TE), 4.0/1.9 ms; flip angle, 18°; slice thickness, 8 mm; field of view (FOV), 380 × 380 mm; matrix, 224 × 224; SR delay time, 200 ms; and sensitivity encoding parallel imaging (SENSE) factor, 2.

The phantom study revealed a correlation between the concentration of Gd-DTPA and MR signal intensity (Fig. 1). We converted the signal to the concentration of Gd-DTPA using the following formula:

$$y = 2E-07X^2 + 8E\text{-}05x - 0.006 \ (r = 1.00), \quad (1)$$

where y is the concentration of Gd-DTPA (μmol/mL) and X is the signal intensity obtained from the phantom data.

Fig. 1

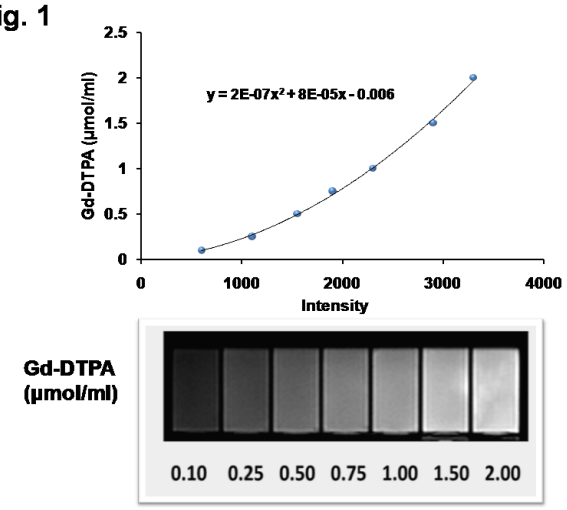

Fig. 1 Relationship between the magnetic resonance signal intensity and the concentration of Gd-DTPA
The lower image is that for the phantom, with several different concentrations (0.10 to 2.0 μmol/mL) of Gd-DTPA in the blood.

MR Perfusion and Delayed Enhancement

For dynamic perfusion, the MRI sequence was obtained using the electrocardiography (ECG)-triggered and breath-hold technique in three short-axis planes (basal, mid-ventricular, and apical). MRI was performed using the same turbo field-echo technique with SR magnetization preparation as described above. Scanning was repeated continuously every two cardiac cycles. The temporal resolution was 160 ms. Gd-DTPA (Magnevist, Bayer, Wayne, NJ) was administered at 0.03 mmol/kg with a flow rate of 4.0 mL/s, followed by a 20-mL saline flush at the same flow rate. The subjects were instructed to hold their breath for as long as possible and take shallow breathes thereafter. The perfusion sequence was initiated concurrently with Gd-DTPA administration. For the stress state, dynamic perfusion MRI was performed 3 min after ATP infusion (160 μg/kg/min), before imaging at rest. After imaging under stress and at rest, additional Gd-DTPA was administered up to a total concentration of 0.1 mmol/kg for late gadolinium enhancement (LGE). An inversion-recovery-prepared fast field echo

pulse sequence was used to obtain a delayed enhancement image for localization of the infarct region in the short axis. The imaging parameters for LGE were as follows: slice thickness, 5 mm; FOV, 380 mm; matrix size, 256 × 256 (512 × 512 reconstructed matrix); TR/TE, 3.0 ms/0.96 ms; flip angle, 10°; and number of signals averaged (NSA), 1. For each subject, we adjusted the inversion time to nullify the signal from the normal myocardium; the typical inversion time was 250 to 290 ms.

Qualitative Analysis of MR Images

One experienced radiologist (16 years of experience with cardiac MRI) assessed the perfusion or late gadolinium enhancement images for the presence of artifacts.

Registration and Analysis of Dynamic Perfusion MR Images

Mutual information maximization was used to correct the respiratory motion of the myocardium[22]. Parallel translation and rotation were performed to minimize entropy around the myocardium. Images of the LV short axis (LVSA) were used to create ROIs. The ROI for the LV blood was manually placed in the left ventricle, and the borders of the inner and outer myocardium were set on the LVSA to obtain TICs for the myocardium. Sample TICs for the pilot group obtained after subtraction of the first frame from all subsequent frames (both at rest and under stress) are shown in Fig. 2. Three coronary segments were defined(Fig. 2), as previously described[6].

Fig. 2

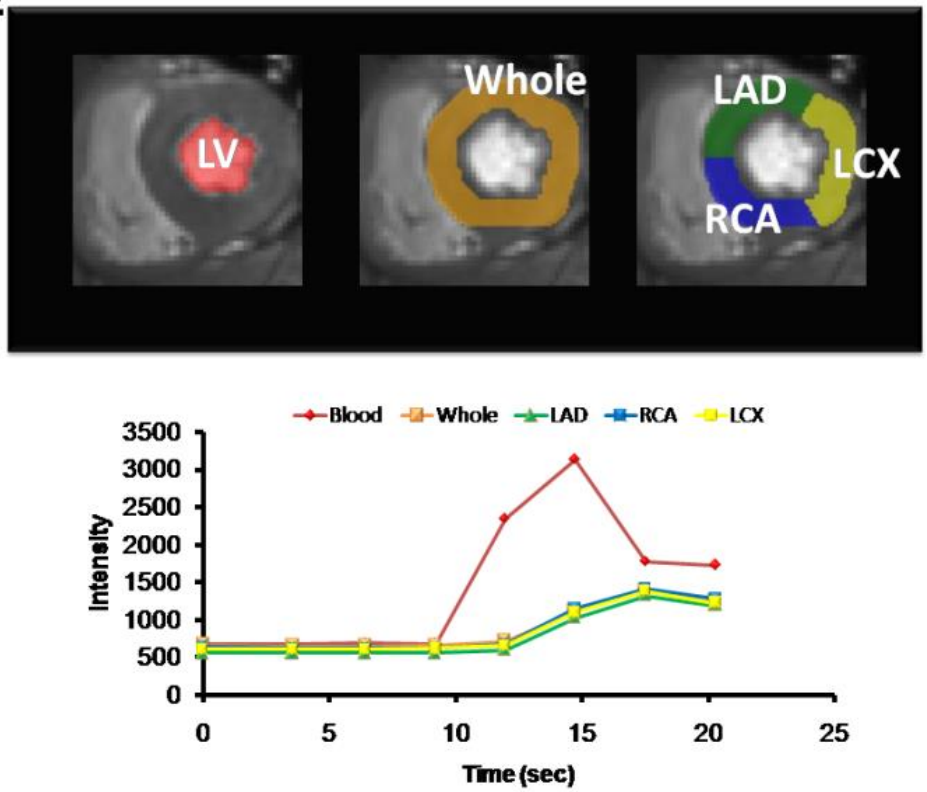

Fig. 2 Time-intensity curves for the left ventricular cavity and myocardium

The regions of interest (ROIs) within the magnetic resonance images of the left ventricular short axis are displayed. Time-intensity curves for each coronary territory and the entire myocardium ROIs are shown.
Relationship between the magnetic resonance signal intensity and the concentration of Gd-DTPA. The lower image is that for the phantom, with several different concentrations (0.10 to 2.0 μmol/mL) of Gd-DTPA in the blood.

MBF_{MRI} Formula with the Single-tissue Compartment Model

Using the formula derived from the phantom study (Eq. 1), we converted the subtracted TIC data to the gadolinium concentrations in the LV myocardium [Ct(t)] and LV chamber [Ca(t)].

Quantitative MBF_{MRI} values were calculated using the single-tissue compartment model and the Renkin–Crone equation[7, 18, 23, 24].

The following equation was used for robust estimation of the K1 value for the contrast medium into Ct(t):

$$dCt(t)/dt = K1 \times Ca(t) - k2 \times Ct(t), \quad (2)$$

where k2 is the outflow rate from the LV myocardium into the LV blood cavity. From the measured Ca(t) and Ct(t) values, $K1_{MRI}$ values were estimated by curve fitting using the nonlinear least-square method. The relationship between MBF and the K1 value for Gd-DTPA was derived using the Renkin–Crone model as follows:

$$K1 = MBF \times E, \quad (3)$$

where E is the extraction fraction specific to a certain tracer or contrast medium. It has a nonlinear relationship with MBF and the product of the effective capillary permeability and surface area (PS, mL/min/g).

$$E = 1 - \exp(-PS/MBF) \quad (4)$$

This model is consistent with the observation that tracer or contrast media extraction typically decreases with flow, despite an increase in PS due to capillary recruitment. The PS function is typically presented following Eq. 5, where s and PS' represent a slope and intercept, respectively.

$$PS = s \times MBF + PS' \quad (5)$$

By combining Eqs. 4 and 5, the extraction function is expressed by the following Eq. 6. In this equation, α and ß represent exp(s) and PS', respectively.

$$E = 1 - \alpha \cdot \exp(-ß/MBF) \quad (6)$$

Using Eqs. (3)and (6), the Renkin–Crone formula was expressed as

$$K1 = MBF \times [1 - \alpha \cdot \exp(-ß/MBF)], \quad (7)$$

Parameters α and ß were estimated using K1 values obtained from perfusion MRI and MBF values obtained from ^{15}O-water PET with the nonlinear least-square method for the first 10 subjects (pilot group).

Patlak Plot Method

We tested K1 values obtained using the Patlak plot method (K1Patlak) as previously

reported[15] and compared them with those obtained using our new method. K1Patlak was estimated using Eq. 8, where R(t) is a curve for the myocardial tissue and LV(t) is a curve for the blood pool.

$$\text{K1Patlak} = \frac{\text{R(t)}}{\int_0^T \text{LV(t)dt}} \quad (8)$$

Statistical Analysis

All data are expressed as means ± SDs. We compared background data such as age, body mass index (BMI), and time interval between MRI and PET examinations between the pilot and validation groups using t-test. Fisher's exact test was used to compare smoking and family history. The rate pressure product (RPP) at rest and the percentage change in heart rate (HR) induced by ATP stress were compared between the rest and stress conditions of MRI and ^{15}O-H_2O PET using t-tests. We used Pearson's correlation coefficients and linear regression analyses with Bland–Altman plots to evaluate the concordance between MBF_{MRI} and MBF_{PET} values. To evaluate the interobserver reproducibility for MBF_{MRI} and CFR_{MRI}, we used Bland–Altman plot analysis, linear regression curves, the coefficient of variability (CV),and intraclass correlation coefficients (ICCs).MBF and CFR values derived by our method were compared with those estimated by the Patlak plot method using Fisher's z transformation. Overall and regional MBF and CFR values were compared between the healthy subjects and CAD patients and between PET and each MRI method using t-tests. A *P*-value of <0.05 was considered statistically significant. JMP ver. 10 (SAS Institute, Cary, NC) was used for all data analyses.

Results

All 20 subjects completed the MRI and PET protocols without experiencing any adverse effects. There were no significant differences in age, BMI, smoking history, blood sample data, and time intervals between PET and MRI examinations between the pilot and validation groups (Table 1). Compared with the subjects in the validation group, patients in the CAD group were older, showed a higher frequency of smoking, and had higher systolic blood pressure, fasting blood sugar (FBS), and glycated hemoglobin (HbA1c) values. No artifacts were observed on the MR perfusion images. No LGE segments were observed in both the healthy subjects and CAD patients.

Table 1. Background characteristics of the 20 healthy male volunteers and 10 patients with coronary artery disease

	Pilot Group (n=10)	Validation Group (n=10)	P-value	CAD Group (n =10)	P-value
Age (year)	28.4 ± 8.9	28.5 ± 8.8	0.98	67.2± 7.8	< 0.001
Gender (male/female)	10/0	10/0	1.00	6/4	0.025
BMI (kg/m^2)	22.3 ± 3.5	21.8 ± 3.4	0.64	23.1 ± 2.6	0.34
Smoker/Non Smoker	4/6	3/7	0.64	8/2	0.024
MRI and PET interval (days)	13.3 ± 8.4	11.9 ± 8.8	0.71	-	
Systolic BP (mmHg)	123.1 ± 9.7	116.7 ± 6.4	0.1	140.3 ± 21.5	0.004
Diastolic BP (mmHg)	71.3 ± 6.5	72.0 ± 6.5	0.81	81.9 ± 14.7	0.08
Heart rate (bpm)	62.1 ± 7.2	63.3 ± 10.3	0.77	66.2 ± 13.3	0.59
T-CHO (mg/dl)	178.8 ± 32.5	174.2 ± 39.3	0.78	189.5 ± 46.7	0.44
HDL-CHO (mg/dl)	54.6 ± 10.8	55.6 ± 7.4	0.81	45.2 ± 11.7	0.03
LDL-CHO (mg/dl)	111.0 ± 27.6	101.3 ± 40.2	0.54	115.1 ± 40.8	0.46
FBS (mg/dl)	83.3 ± 7.3	88.9 ± 6.5	0.09	147.7 ± 41.5	< 0.001
HbA1c (%)	5.12 ± 0.28	5.12 ± 0.33	0.94	6.43 ± 0.81	< 0.001
Vessel disease (N)					
1-VD				7	
2-VD				1	
3-VD				2	

BMI; body mass index (kg/m^2) , T-CHO; total cholesterol (mg/dl), HDL-CHO; high-density lipoprotein cholesterol (mg/dl), LDL-CHO; low-density lipoprotein cholesterol (mg/dl), FBS; fasting blood sugar (mg/dl), HBA1c; hemoglobin A1c (%); P-values between pilot and validation groups, and between validation and CAD groups

Hemodynamic Parameters at Scanning

HR and RPP values for the pilot and validation groups showed similar and significant increases from the resting state to the ATP-induced stress state ($P < 0.001$) in both MRI and PET studies (Table 2).

Table 2. Hemodynamic parameters at MRI and PET scans

		Pilot set (n=10)			Validation set (n=10)		
		MRI	PET	P-value	MRI	PET	P-value
Rest	HR	62.1 ± 7.2	65.3 ± 11.6	0.70	63.3 ± 103	60.6 ± 7.2	0.52
	SBP	123.1 ± 9.7	124.2 ± 9.1	0.71	116.7 ± 6.4	121.9 ± 10.4	0.17
	DBP	71.3 ± 6.5	71.3 ± 12.5	0.94	72.0 ± 6.5	69.2 ± 8.5	0.50
	RPP	7664 ± 1232	8126 ± 1628	0.65	7395 ± 1325	7416 ± 1304	0.94
Stress	HR	81.4 ± 8.9	80.7 ± 9.4	0.32	85.8 ± 13.0	80.3 ± 9.8	0.47
	SBP	120.0 ± 7.5	115.6 ± 9.4	0.36	113.8 ± 5.9	112.4 ± 10.5	0.50
	DBP	68.5 ± 5.2	65.9 ± 13.5	0.71	68.0 ± 6.1	63.3 ± 8.0	0.17
	RPP	9791 ± 1394	9370 ± 1541	0.50	9780 ± 1705	9025 ± 1344	0.65

HR; heart rate (bpm), SBP; systolic blood pressure (mmHg), DBP; diastolic blood pressure (mmHg), RPP; rate pressure product (bpm*mmHg)

Extraction Fraction for the Pilot Group

Fig. 3 shows the relationship between $K1_{MRI}$ and $K1_{PET}$ values estimated from the pilot group data. We estimated the parameters α (0.892) and β (0.964) using Eqs. (3)–(7). The Renkin–Crone formula between $K1_{MRI}$ and MBF_{MRI} was expressed as follows.

$$K1 = MBF \times [1 - 0.892 \cdot \exp(-0.964/MBF)]$$

This equation was used to calculate MBF_{MRI} values for the validation and CAD groups using the $K1_{MRI}$ value for each subject.

Fig. 3

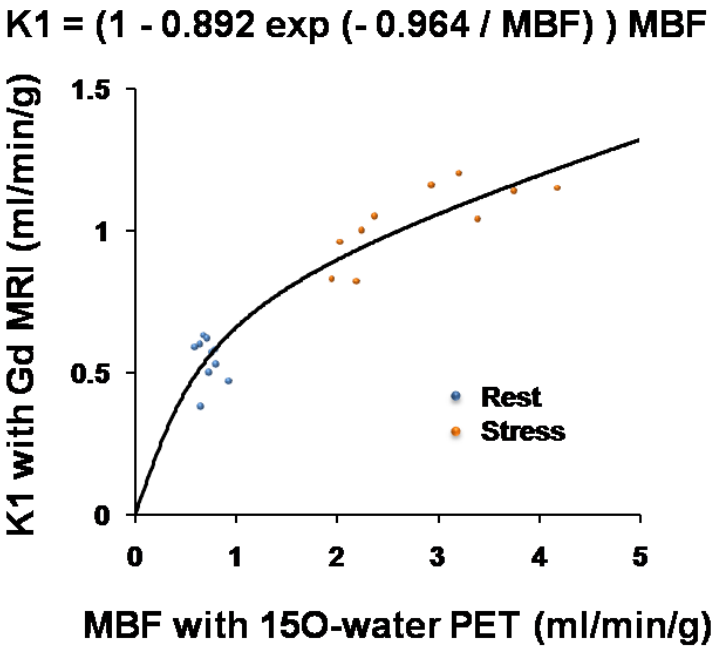

Fig. 3 Relationship between K1 values obtained using MRI and myocardial blood flow (MBF) obtained using ^{15}O-water PET in the pilot group

The black circles represent the rest condition and the white circles indicate the stress condition.

Validation of MBF_{MRI} and CFR_{MRI} Values against MBF_{PET} and CRF_{PET} Values

In the overall LV analysis, resting MBF_{MRI} and stress MBF_{MRI} values were 0.76 ± 0.10 mL/min/g and 3.04 ± 0.82 mL/min/g, respectively, while the corresponding PET values were 0.71 ± 0.11 mL/min/g and 3.09 ± 0.97 mL/min/g, respectively (Table 3). A significant relationship was confirmed between MBF_{MRI} and MBF_{PET} values (Fig. 4a) and between CFR_{MRI} and CFR_{PET} values in the validation group (Fig. 5a). The three regional per-vessel analyses for MBF and CFR showed a similar trend (Table 3, Figs. 4b and 5b).

The variability in MBF between the two independent observers is shown in Fig. 6a strong interobserver correlation was observed (ICC, 0.98 for the overall analysis and r = 0.97 for the regional analysis).

Fig. 4

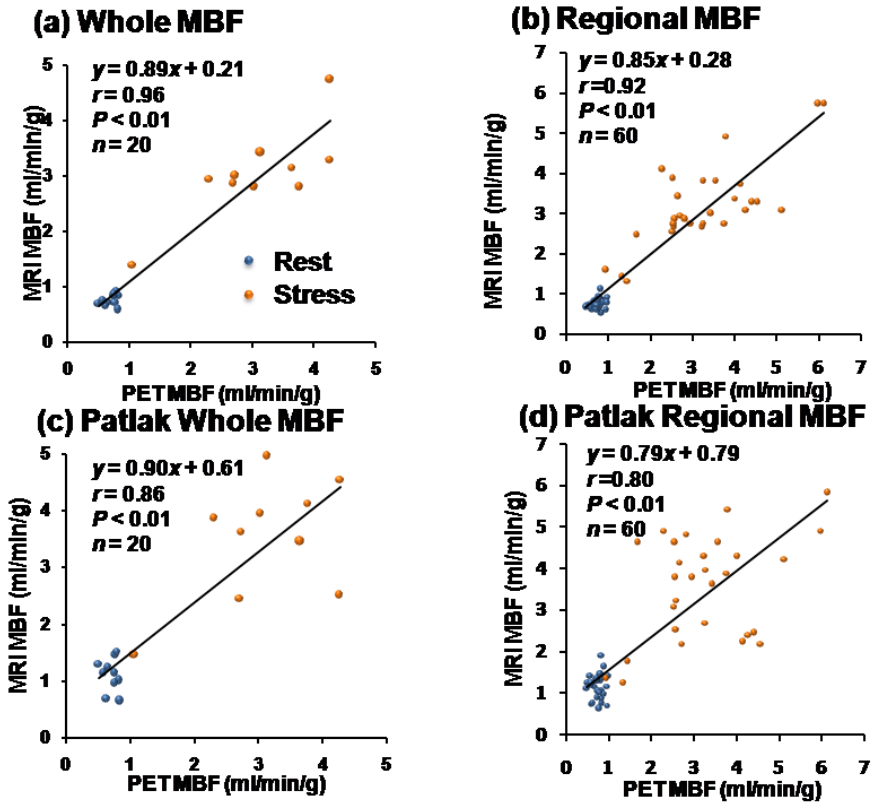

Fig. 4 Comparison between MBF_{MRI} and MBF_{PET} values: the single-tissue compartment model vs. the Patlak plot method

Our new method using the single-tissue compartment model reveals significant correlations with ^{15}O-water PET in both the overall and regional analyses (a and b). Comparisons of the findings with those of the Patlak plot method are also demonstrated (c and d).

Fig. 5

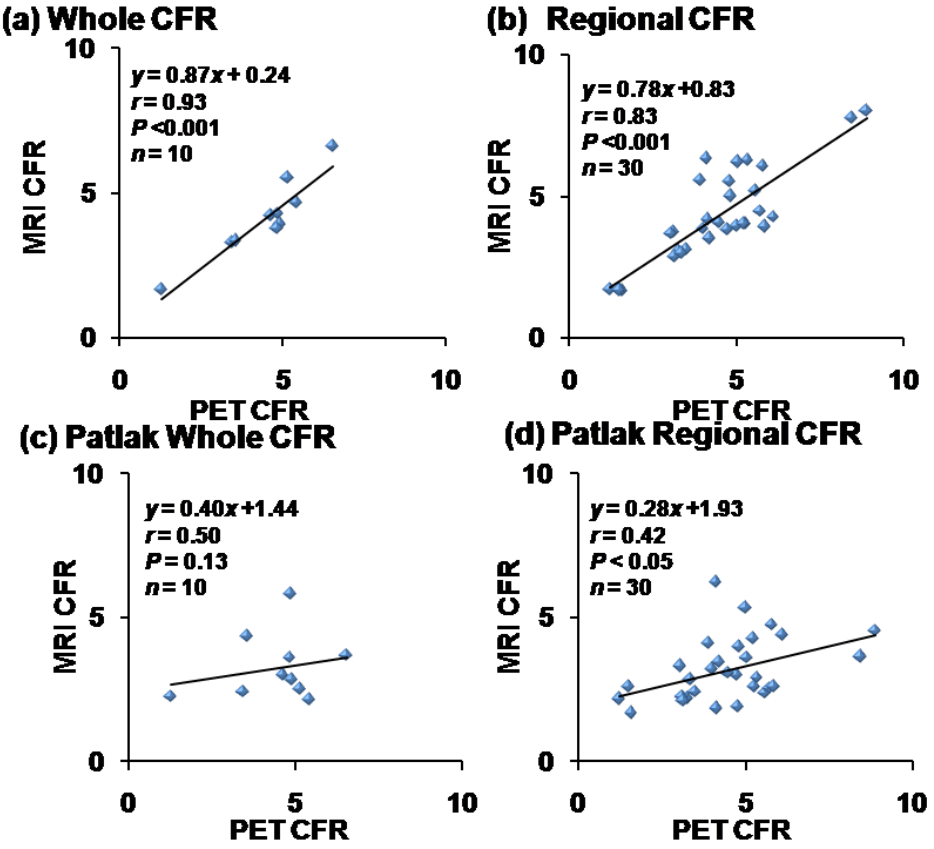

Fig. 5 Comparison of CFR_{MRI} and CFR_{PET} values: single-tissue compartment model vs. the Patlak plot method

Our new method using the single-tissue compartment model shows better correlations with ^{15}O-water PET in both the overall and regional analyses (a and b) compared with the Patlak plot method (c and d).

Fig. 6

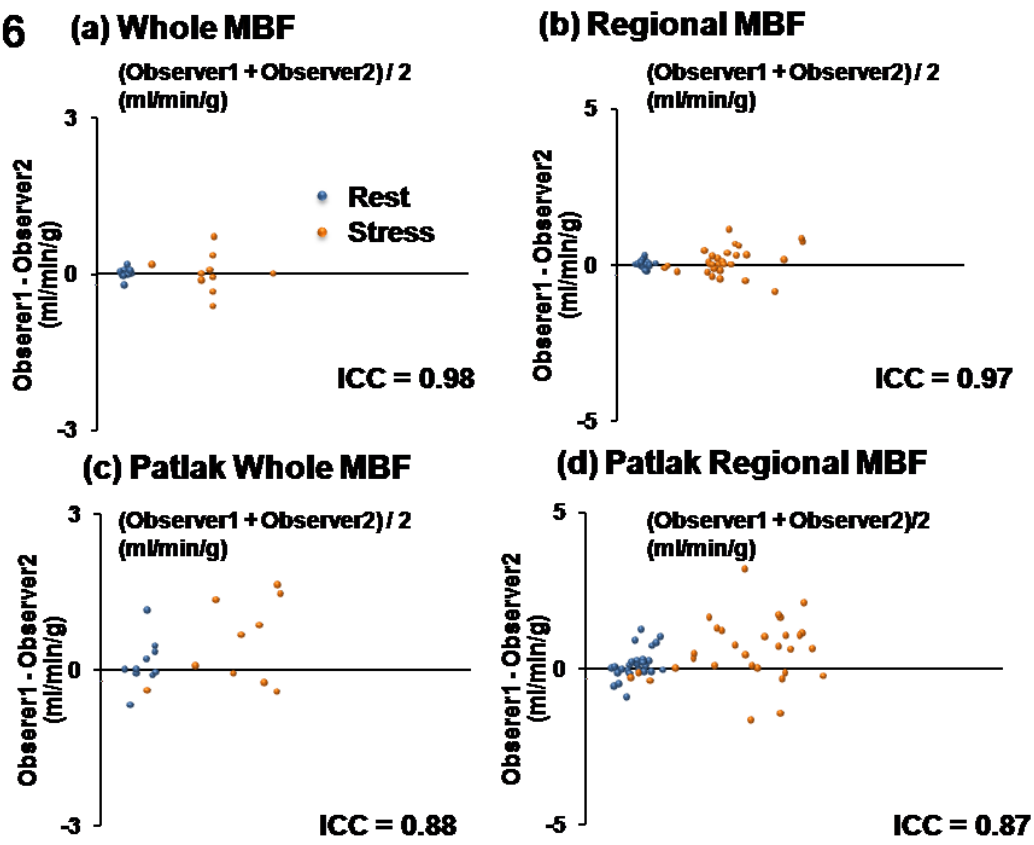

Fig. 6 Bland–Altman plots for interobserver variability in the validation group

A strong interobserver correlation is observed with our new method (a and b), with higher ICC values for our method than for the Patlak plot method (c and d).

Table 3. Comparison of the whole and regional MBF and CFR between PET and MRI

		^{15}O-water PET	MRI Single Compartment	MRI Patlak
Rest MBF	Whole	0.71 ± 0.11	0.76 ± 0.10	1.10 ± 0.29**
	LAD	0.73 ± 0.13	0.78 ± 0.16	1.12 ± 0.29**
	LCX	0.79 ± 0.13	0.75 ± 0.11	1.26 ± 0.26**
	RCA	0.68 ± 0.11	0.75 ± 0.12	1.08 ± 0.28**
Stress MBF	Whole	3.09 ± 0.97	3.04 ± 0.82	3.49 ± 1.07
	LAD	3.35 ± 1.25	3.31 ± 1.20	3.47 ± 1.26
	LCX	3.73 ± 1.31	3.24 ± 1.11	3.84 ± 1.29
	RCA	2.69 ± 1.01	2.96 ± 0.76	3.47 ± 1.31
CFR	Whole	4.46 ± 1.43	4.13 ± 1.33	3.25 ± 1.14
	LAD	4.68 ± 1.84	4.37 ± 1.79	3.17 ± 1.15*
	LCX	4.81 ± 1.87	4.39 ± 1.65	3.11 ± 0.94*
	RCA	4.04 ± 1.47	4.10 ± 1.37	3.27 ± 1.30

MBF; myocardial blood flow, CFR; coronary flow reserve, LAD; left descenging artery, LCX ; left circumflex artery, RCA ; right coronart artert, unit of MBF is mL/g/min, t-test between PET and MRI * ; $P < 0.05$; ** $P < 0.01$

Comparison of Overall and Regional MBF_{MRI} and CFR_{MRI} Values between the Healthy Subjects and CAD Patients

The overall stress MBF_{MRI} and CFR_{MRI} values were significantly lower in the CAD group than in the healthy group (Fig. 7a and 8a). The regional stress MBF_{MRI} and CFR_{MRI} values were significantly lower in the CAD group (>75% stenosis) than in the healthy group (Fig. 7b and Fig. 8b); a similar trend was observed for nonstenotic regional stress MBF_{MRI} and CFR_{MRI} values.

Fig. 7

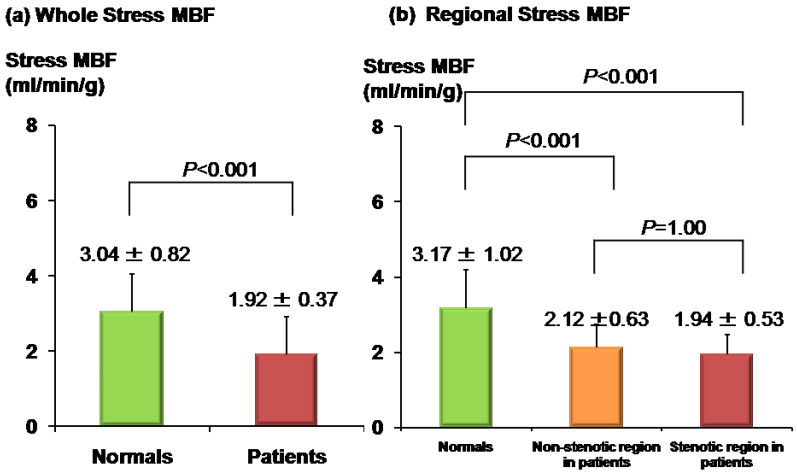

Fig. 7 Comparison of overall and regional MBF values between CAD patients and healthy subjects

The overall MBF value is significantly lower for the CAD patients than for the healthy subjects ($P < 0.001$, 7a); a similar trend is observed for regional MBF_{MRI} values (>75% stenosis; $P < 0.001$, 7b).

Fig. 8

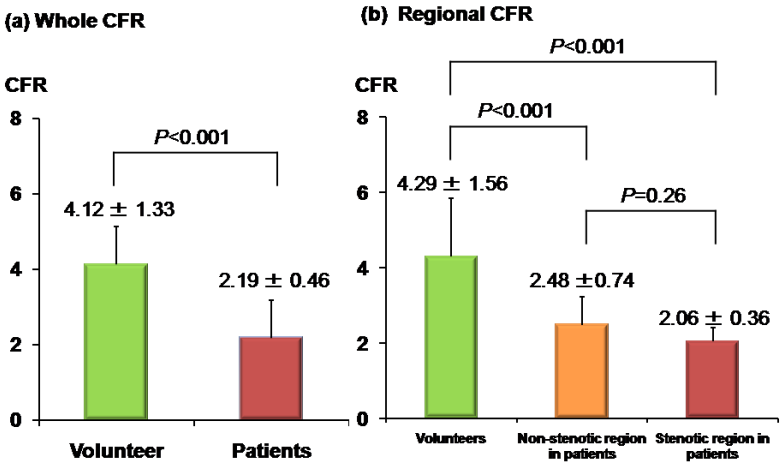

Fig. 8 Comparison of the overall and regional CFR values between CAD patients and healthy subjects

The overall CFR is significantly lower for the CAD patients than for the healthy subjects ($P < 0.001$, 8a); a similar trend is observed for regional CFR_{MRI} values (>75% stenosis; $P < 0.001$, 8b).

Comparison of MBF_{MRI} Values: Single-tissue Compartment Model vs. the Patlak Plot Method

Resting and stress MBF_{MRI} and CFR_{MRI} values obtained using the Patlak plot method are shown in Table 3. These values were significantly correlated with those obtained using ^{15}O-water PET (r = 0.86 and 0.50 in the overall analysis and 0.80 and 0.42 in the regional analysis; Figs. 4 and 5). However, the correlation between values obtained using our method and those obtained using the single-tissue compartment model was significantly better that that between values obtained using our method and those obtained using the Patlak plot method, in both the overall and regional analyses (overall: P = 0.048, regional: P = 0.002). In addition, ICC values (0.88 in the overall analysis and 0.87 in the regional analysis) for the Patlak plot method were lower than those for our method (ICC, 0.98 for the overall analysis and r = 0.97 for the regional analysis). Resting MBF_{MRI} and CFR_{MRI} values obtained using the Patlak plot method were significantly different from PET values, while all MRI values obtained using our method were comparable to PET values (Table 3).

Discussion

We developed a method to estimate the overall and regional MBF values using the single-tissue compartment model and dynamic perfusion MRI at 3T. We calculated the extraction fraction using TICs for perfusion MRI at 3T and compared them with those obtained using ^{15}O-water PET data to estimate Renkin–Crone parameters in the pilot group. The model derived a strong correlation between MBF_{MRI} and MBF_{PET} values in the validation group, suggesting that it accurately quantifies MBF values from dynamic perfusion MRI at 3T. CAD patients exhibited significantly lower overall and regional stress MBF_{MRI} and CFR_{MRI} values compared with the healthy subjects. We also compared our method with the Patlak plot method and demonstrated that our model had better concordance with ^{15}O-water PET.

Several quantitative MBF_{MRI} studies using 1.5T MRI have been reported[12-15, 25]. Some of these reports validated MBF_{MRI} values against NH_3 PET values[13, 14]. ^{15}O-water PET is the gold standard method for the quantitative assessment of MBF, because it is the only method using a freely diffusible tracer with a 100% extraction fraction even under increased blood flow[23]. The extraction fractions for other tracers, such as ^{13}N-ammonia

and ^{82}Rb, are lower than that for ^{15}O-water PET [23]. This study was the first, as per our knowledge, to validate MBF and CFR values calculated using dynamic perfusion MRI at 3T against those calculated using ^{15}O-water PET.

Our 3T MRI quantitative method showed high concordance with ^{15}O-water PET, and regional decreases in MBF_{MRI} and CFR_{MRI} values were observed in areas of coronary artery stenosis. Even the nonstenotic region in CAD patients showed decreased MBF_{MRI} and CFR_{MRI} values compared with those for the healthy subjects; this finding was consistent with those in our previous report[3]. We previously indicated a wide variability in CFR values in relation to coronary artery stenosis despite the lower CFR values in stenotic regions than in nonstenotic regions[3, 6]. We also reported that CFR values obtained using ^{15}O-water PET, even for the nonstenotic regions, was decreased because of multiple risk factors such as diabetes and smoking[6]. The CAD patients in this study, who showed higher FBS and HbA1c values and an increased frequency of smoking compared with the healthy subjects, may have had coronary microcirculation dysfunction, resulting in decreased CFR values for the nonstenotic regions. Further prospective studies with a larger patient sample are warranted to assess the relationship between CFR and coronary stenosis using MRI.

The single-tissue compartment model for quantitative MRI perfusion used in the present study showed a better correlation with ^{15}O-water PET (Fig. 4 and 5) and a higher interobserver reproducibility (Fig. 6) compared with the Patlak plot method. Quantitative analysis of absolute MBF requires measurement of the entire dynamic contrast curve [26]. The Patlak plot method is more suitable for the analysis of shorter durations (6 to 10 s) in a dynamic dataset, and theoretically, it may not be useful for the analysis of longer entire dynamic perfusion durations[15, 26]. Hsu et al. used the single-tissue compartment model for the calculation of MBF without consideration of the k2 value[27]. Our method using both K1 and k2 values requires the entire dynamic curve[28] and is more complicated than the Patlak plot method or upslope methods, which do not consider the k2 value. Without consideration of the k2 value, systematic overestimation of MBF values can occur, particularly at high flow[28]. We therefore believe that our method, which uses both the K1 and k2 values, is more complicated but more physiological for calculating MBF. In fact, our method corrected the extraction fraction, even at high flow, with the Renkin–Crone formula using ^{15}O-water PET, which is the gold standard and the best tracer, as the reference and showed better results than those from the Patlak plot method.

On setting the ROIs for the LV blood and myocardium, motion artifacts may occur because of body movement or various gate timings. Motion artifacts can cause mixing errors of signals between the blood and myocardium. We previously developed the mixing correction method (7,18), which considered the overwrapping ratio between parameters in the LV cavity and myocardium [Ca(t) and Ct(t)] and calculated them using the nonlinear least-square method. This model could compute a more accurate myocardial tissue curve with lesser errors due to artifacts.

This study had some limitations. First, the order of imaging at rest and under stress differed between the two modalities. In our MRI protocol, imaging under stress perfusion was performed first, followed by that at rest. In ^{15}O-water PET, imaging was performed in the reverse order to save time. However, we contend that the difference in scan order between MRI and ^{15}O-water PET did not significantly affect the results, because RPPs were not significantly different between the two modalities and a previous study showed that this difference in scan order did not affect MBF_{PET} values[29]. In addition, we subtracted the first frame image from all the other images in both the stress and rest conditions and calculated the inflow rate from the subtracted images. We therefore believe that the effect of the remaining Gd-DTPA injected at the time of imaging under stress perfusion did not affect the images obtained at rest.

Second, the relaxivity of Gd-DTPA depended on the temperature, and our ex vivo phantom results at room temperature may have overestimated the quantitative values because of a relatively lower temperature[30]. However, for perfusion, we administered the contrast agent at room temperature without warming, and the relaxivity of the contrast medium at the first pass in vivo may not have been strongly affected.

Third, this study did not include patients with myocardial infarction. Our model can be used for viable myocardium without myocardial infarction. However, the major objective of this study was to quantify MBF_{MRI} values in comparison with those obtained using the well-documented ^{15}O-H_2O PET technique. For myocardial infarction, we should consider the effects of late gadolinium enhancement on quantitative analysis.

Conclusion

We developed and validated the single-tissue compartment model to estimate MBF using dynamic perfusion MRI at 3T. MBF_{MRI} values showed high reproducibility and a strong correlation with MBF_{PET} values in the healthy subjects. Furthermore, MBF_{MRI} and CFR_{MRI} values were lower for the CAD patients than for the healthy subjects. This method is expected to demonstrate a wide range of applications in various patient populations.

Chapter 2

Quantitative Measurements of Brachial Artery Vascular Function Using Automated Oscillometric Methods Comparison with Ultrasound

Yuuki Tomiyama, Keiichiro Yoshinaga, Satoshi Fujii,Noriki Ochi, Mamiko Inoue, Mutumi Nishida, Kumi Aziki,Tatsunori Horie, Chietsugu Katoh and Nagara Tamaki

Introduction

Arterial diameter enlargement is thought to be an early indicator in the progression of atherosclerosis[31, 32]. Increasing brachial artery diameter is related to conventional cardiovascular risk factors[33]. Brachial artery ultrasound has been used to obtain this measurement and is considered to be the standard measurement. However, data acquisition and data analysis require experienced operators, and therefore an alternative simple automated measurement approach should be developed.

Functional deterioration appears before the development of anatomical vascular changes[34-36]. Arterial elastic mechanics are linked to arterial stiffness[37-39]. Determination of arterial diameter at very low or zero transmural pressure (TP) makes calculation of vessel strain and volume elastic modulus (V_E) possible[40]. Some studies have estimated the V_E in different approaches. Bank et al estimated this marker using a water-filled blood pressure (BP) cuff with an external ultrasound[40]. Kinlay et al estimated this marker using intravascular ultrasound and a catheter[41]. Both approaches measured vascular area changes during various pressure changes. Kinlay et al obtained intra-arterial pressure from the side arm of the arterial sheath, and Bank obtained arterial pressure information using applanation tonometry. These earlier approaches were either complex or invasive, and so a simple noninvasive V_E measurement that could be widely used in clinical settings was sought. Recently, we developed a new automated oscillometric method to measure a brachial artery's estimated area (eA) and V_E. The main

control unit created various fixed precise volumes of air, which are capable of changing the tube size, giving rise to the so-called tube law[42]. Changing tube size may be associated with vascular cross-sectional area. Differences between intramural blood pressure (BP) and cuff pressure (CP) can be obtained using oscillometric measurements. This is the fundamental concept of this automated system. Using the pressure-volume curves, this oscillometric method quantitatively estimates eA and V_E. Preliminary data by Otsuka el al[43] showed a close relationship between eA and cardiovascular risk factors during health checkups. However, this approach has not been validated using other standard measurements, and its reproducibility has not been evaluated.

The aim of this study was to investigate the reliability of the new automated and quantitative oscillometric measurement of eA and V_E. Therefore, we compared eA to ultrasound measurements as a standard and evaluated the reproducibility of these measurements.

Material and Methods

Study subjects

Sixteen volunteers participated in the study. Volunteers were recruited from our Hokkaido University Hospital staff members, postgraduate school of medicine staff members and department of Health Sciences, Hokkaido University staff members. All participants were men and 2 participants were cigarette smokers. All participants had a normal resting electrocardiogram and did not have a history of cardiovascular disease. They were not taking any cardiac medications. Fourteen healthy control subjects had a low pre-test likelihood of coronary artery disease (CAD) (< 5%) based on risk factors[44].

Among 16 healthy individuals, 8 subjects less than or equal to 35 years of age were classified as the younger group. The remaining 8 who were greater than 35 years of age were categorized as the older group[45].

The study was approved by the Hokkaido University Graduate School of Medicine Human Research Ethics Board. Written informed consent was obtained from all subjects.

Study protocol

We evaluated vascular function using brachial artery ultrasound and automated oscillometric methods at rest and after sublingual nitroglycerin (NTG) administration.

In the ultrasound study, we obtained data at rest, after flow-mediated dilatation (FMD), and after NTG administration. However, we used only rest and NTG stress data in the current study because we did not perform reactive hyperemia for oscillometric measurements.

We also performed oscillometric measurements twice, on different days, to evaluate the reproducibility of this automated technique. These measurements were performed in randomized order. All examinations were performed within a three-week period.

We obtained blood samples on the day of the first oscillometric measurements.

Blood sampling and biochemical measurements

We performed venous blood sampling after the oscillometric measurement under overnight fasting conditions[46, 47]. Fasting blood sugar (FBS) was measured using the glucose oxidase method. Serum cholesterol and triglycerides were measured using standard enzymatic methods. HDL cholesterol concentration was measured from the serum supernatant after precipitation of very low density lipoprotein and LDL subfraction. LDL cholesterol was calculated by the Friedewald formula[48].

Brachial artery ultrasound measurements with flow-mediated vasodilatation: Subject preparation

Participants were instructed to abstain from caffeine-containing products (coffee, tea, chocolate, cola) for at least 24 hours and vitamin C-containing beverages for at least 6 hours[35]. They fasted $\geq$8 hours (overnight fasting) prior to the ultrasound measurements[41, 49]. Two smokers were instructed to abstain from smoking for at least 12 hours in order to minimize acute smoking effects. The ultrasound study was conducted in the morning (8 a.m.) after overnight fasting(Fig. 1a). Subjects rested in a supine position for 10 minutes before the study in a temperature-controlled room (21℃ to 23℃). An automated sphygmomanometer cuff was positioned on the left arm for measurement of BP[41].

Fig. 1

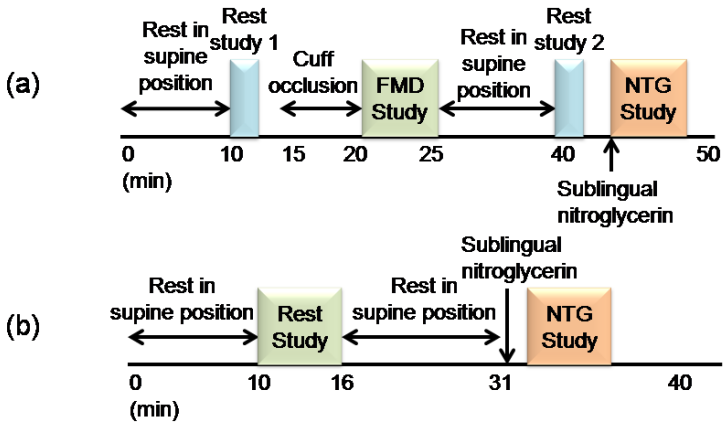

Fig. 1 Study design

(a) Data acquisition protocol of ultrasound measurements
(b) Data acquisition protocol of oscillometric measurements

Image acquisition

High-resolution Doppler ultrasonography equipment (Aplio XG, Toshiba, Tokyo, Japan) with an 18-MHz transducer was used to evaluate the right brachial artery. The onset of the R wave was used to identify end-diastolic vascular diameter, and the peak of the T wave was used to identify end-systolic diameter[50].

The brachial artery was longitudinally scanned approximately 5 cm above the antecubital fossa. We also evaluated brachial artery diameter 8.5 cm above the antecubital fossa before the standard rest measurement, which was 5 cm above the antecubital fossa, in order to compare oscillometric measurements. After an appropriate probe position was determined, the skin was marked and the arm was retained in the same position throughout the study. The echo transducer was supported by a stereotactic probe-holding device.

After 10 minutes of rest in a supine position, brachial artery diameter was measured at rest as a baseline study.

Endothelium-independent vasodilatation with nitroglycerin

Fifteen minutes after the FMD study, a new baseline image was obtained. After the second baseline data acquisition, subjects received 0.3 mg of sublingual NTG (TOA EIYO, Fukushima, Japan). Just after sublingual NTG administration, brachial artery image acquisition was started and continued for 5 minutes[41].

Image analysis

Brachial artery diameter was measured from the anterior to the posterior medial-adventitial interface at the end-diastole. We evaluated the vascular diameter for 4 cardiac cycles and calculated the mean value. The means of the two measurements by independent observers were calculated. The inter-operator reproducibilityof ultrasound measurement in our facility had an ICC of 0.92. The percentage increase of diameter by nitroglycerin (%NTG) was calculated as follows[51]:

%NTG = brachial artery diameter at NTG stress / average of baseline diameter × 100.

Automated vascular volume/pressure detector measurements: Oscillometric measurement protocol

Subjects followed the same instructions they had received for ultrasound measurements prior to the studies. Participants underwent oscillometric measurements after overnight fasting. We performed rest brachial arterial cross-sectional area and functional measurements using a newly developed device, the Health Chronos TM-2771 prototype (A&D Company, Limited, Tokyo, Japan) (Fig. 2a)[43]. Data acquisition took 6 minutes (Fig. 1) and included measurements of BP, eA, and V_E (i.e. vascular stiffness). After the rest data acquisitions, participants rested for 15 minutes. Then, subjects received sublingual NTG (0.3 mg). Two minutes after sublingual NTG administration, the second measurements were performed (Fig. 1b).

Fig. 2a

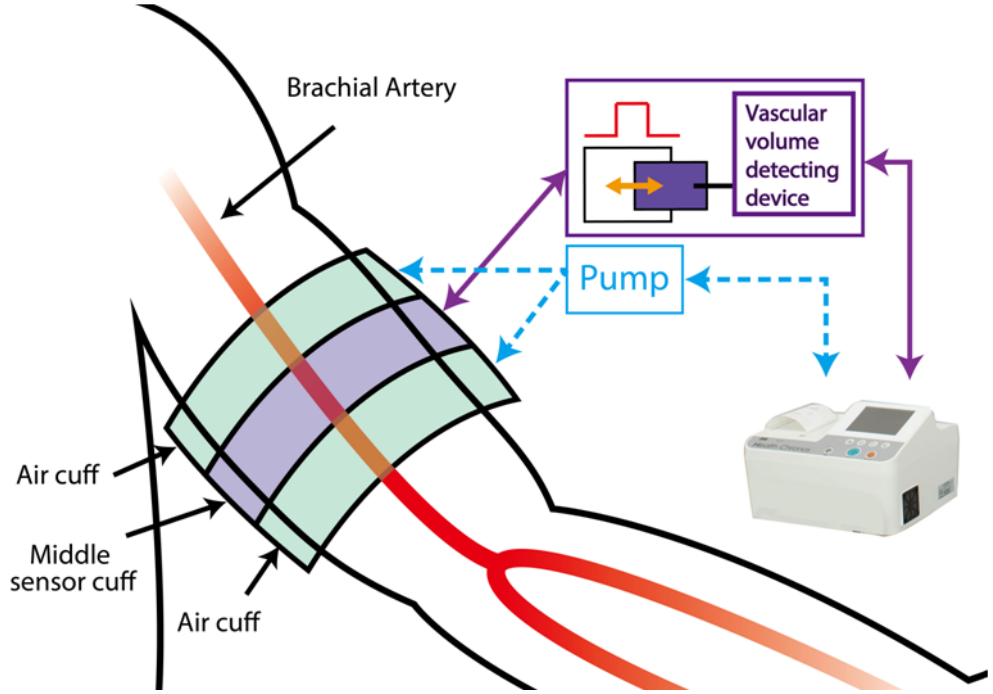

Fig.2a Oscillometric measurements set-up.

A triple lumen cuff was put on the upper arm. The triple lumen cuff included central pressure sensor cuff and two outside cuffs. The central part of the triple lumen cuff detected the exact vascular volume change. A main control unit generated a precise amount of air into all 3 cuffs. After sending the precise amount of air, two tubes to the outside cuffs were occluded. These amounts of air changed the vascular volume and added a stable pressure to the vessel.

After sending the air, the main controlunit changed a valve connection to the central cuff and the central cuff changed its role. The central cuff then sensed the vascular volume change and controlled thecuff pressure.

The central pressure sensor cuff detected BP-CP differences during heartbeats. Using this information, the main control unit made pressure-volume curves.

Data analysis

We measured brachial artery absolute volume and V_E using a newly developed device, the Health Chronos TM-2771 prototype. Details of this device are addressed elsewhere[43]. In brief, this device consists of a main control unit and two outside cuffs for oscillometric measurement and plethysmography at the right and left brachial arteries (Fig. 2a). The exteriors of the 3 occlusive lumen cuffs are composed of a hard material to avoid expansion with increases in arterial volume. Therefore, the - cuff pressure (CP) changes accurately reflected volumetric changes of the brachial artery. To measure a brachial artery's absolute volume, the device initially sought the lowest CP that indicated complete occlusion of the brachial artery (volume = 0) at end-diastole. During the measurement, the main control unit put air into the central cuff for a calibration. This calibration made it possible to determine the absolute volumetric changes of the brachial artery from the plethysmogram under the condition of outside cuff inflation. The CP was gradually decreased and the calibrated plethysmogram was recorded several times at regular CP intervals. Thus, pressure and area curves were obtained.

To estimate the cross-sectional area of the brachial artery, the brachial arterial volume was divided by the length of the central cuff, which was a pressure-sensor cuff.

The eA was defined as the estimated cross-sectional area at the point where the BP-CP difference was identical to the diastolic BP (Fig. 2b). The highest CP, indicating complete collapse of the brachial artery, is usually a little higher than BP. Therefore, the corresponding point (P0) on the pressure axis of the curve was set at less than zero.

$V_E$was defined as the change in the BP-CP difference (DP1) per 1% increase in cross-sectional area at P1, where P1 = P0 + 40 mm Hg. The original calculation of V_E was as follows [52] [V_E =Δ Pressure/ (100 × ΔVolume/ Volume) mmHg/%]. This system estimated the absolute value of cross-sectional vascular area instead of vascular volume. Thus, the original V_E equation was modified as follows[43] [V_E =Δ Pressure/ (100 × ΔArea/ Area) mmHg/%]. The principal concept of V_E estimation was to evaluate the association between ΔA and ΔP while the blood vessel remained circular. The correct measurements should be performed with cuff pressure below a certain point so that the vessel remains circular and does not have buckling. Based on our basic preliminary experimental laboratory data analysis, in most cases vessels remained circular when pressure was 40 mm Hg higher than P0.

Although we obtained the values of eA and V_E for both right and left brachial arteries, the values for eA and V_E for the right brachial artery were used in the subsequent statistical analysis since the ultrasound measurements we performed were for the right brachial artery.

The percentage increase of eA and V_E with nitroglycerin (%NTG) was calculated as follows: %NTG = eA or V_E at NTG stress / rest eA or V_E × 100

The measurement was similar to that obtained using ultrasound.

Fig. 2b

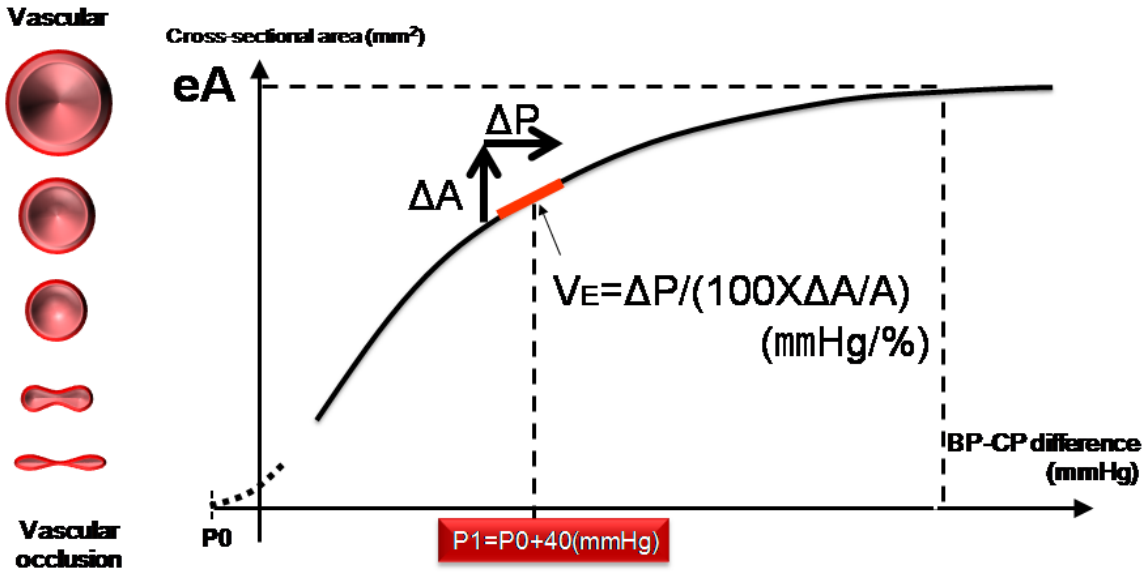

Fig.2b Calculation of estimated cross-sectional area (eA) and volume elastic modulus (V_E) using pressure-volume curves.

When cuff pressure became zero, the calculated cross-sectional vascular area represented baseline vascular area.

Statistical analysis

Continuous variables were presented as means and standard deviations. Categorical data were expressed as a percentage of total. The paired Student's t-test and unpaired Student's t-test were used for continuous variables. Pearson's correlation coefficient was analyzed to determine the simple correlation between variables. In the analysis, all statistical tests were two-sided. A *P*-value of less than 0.05 was considered indicative of a statistically significant difference. The reliability of oscillometric measurement was assessed using an ICC. The strength of the ICC was determined using the cutoffs of 0.5, 0.3 and 0.1 for high, moderate and low levels of agreement according to Cohen's effect size convention[52]. Statistical calculations were carried out using SAS software version 9.2 (SAS Institute, Inc., Cary, NC).

Results

Reliability of oscillometric measurements

Subject characteristics.

Baseline characteristics of the 16 subjects are shown in Table 1a. Among 16 individuals, 2 subjects were cigarette smokers. Lipid profiles, including total cholesterol and low density cholesterol, FBS, and HbA1c, were within normal range. The interval between the ultrasound and oscillometric measurement was 4.9±3.7 days.

Table1a. Baseline characteristics

	Subject (n= 16)
Normal/Smoker	14/2
Age (years)	35.2±13.1
Height (cm)	169.4 ± 4.4
Weight (kg)	68.0±9.2
BMI (kg/m^2)	23.7 ± 3.2
Systolic BP (mmHg)	115.2±15.1
Diastolic BP (mmHg)	72.5±11.7
HR (bpm)	62.1±9.8
T-CHO(mg/dl)	199.3±39.9
LDL-CHO(mg/dl)	119.1±62.9
FBS(mg/dl)	88.3±8.7
HbA1c(%)	4.9±0.2

BMI; body mass index (kg/m^2),BP; blood pressure (mmHg),HR; heart rate (bpm), ;T-CHO; total cholesterol (mg/dl),LDL-CHO; low-density lipoprotein cholesterol (mg/dl)FBS; fasting blood sugar (mg/dl); HbA1c, haemoglobin A1c (%)

Association between ultrasound measurements and oscillometric measurements

Ultrasound showed upper-arm brachial artery diameter 8.5 cm above the antecubital fossa as 3.93±0.49 mm. Vascular cross-sectional area measured by oscillometric measurement was 12.3±3.0 mm^2. This value was converted to diameter (3.97±0.51 mm) for comparison to ultrasound measurements. There was no difference in brachial vascular diameter between ultrasound and oscillometric measurement (P = 0.65). Brachial vascular diameter derived from oscillometric measurements significantly correlated with ultrasound brachial artery diameter measurements (r = 0.75, P< 0.001, Fig. 3).

Fig. 3

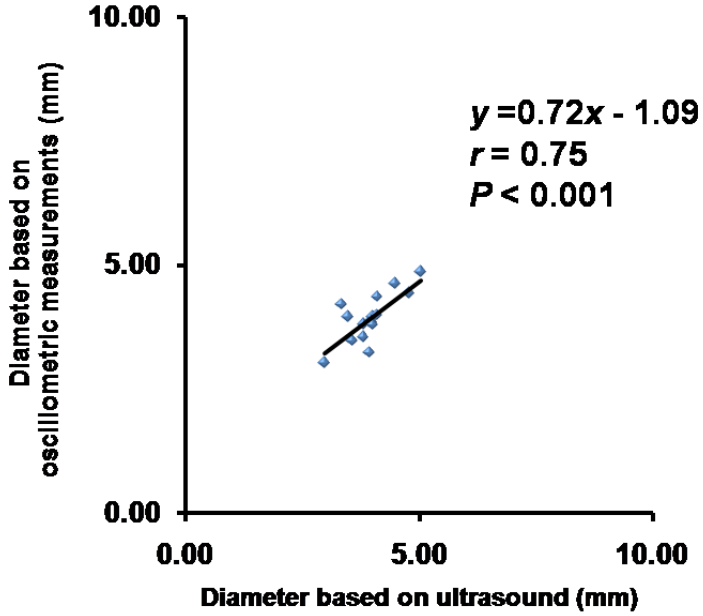

Fig. 3 Correlation between ultrasound measurements and oscillometric measurements of rest brachial artery diameter.

Rest eA was converted to vascular diameter.

Rest reproducibility of eA and V_E measurements

All 16 subjects had two oscillometric measurements. The mean interval between the two oscillometric measurements was 7.2±5.2 days. There was no significant difference in subjects' baseline condition between the first and second study including height (P= 0.33), weight (P= 0.32), systolic BP (P= 0.64), diastolic BP (P= 0.35) or heart rate (P= 0.67). There was no significant difference in rest eA (11.9±3.0 vs. 11.5±2.9 mm^2, P = 0.32) or V_E(0.82±0.16vs. 0.77±0.16 mm Hg/%, P= 0.09) between the first and second studies. Rest eA and rest V_E showed good reliability (eA: ICC = 0.88, V_E: ICC = 0.78).

Nitroglycerin stress responses

NTG administered sublingually significantly decreased systolic BP (115.2 ± 15.1 to 108.2±13.9 mm Hg, $P = 0.0004$) and increased heart rate (HR) (62.2 ± 9.8 to 67.8 ± 7.2 bpm, $P = 0.002$) in oscillometric measurements.

Ultrasound showed increasing arterial diameter after NTG administration (4.46 ± 0.72 to 4.73± 0.75 mm, $P<0.001$). The percentage change of arterial diameter with NTG was 15.7±5.0 %. eA was significantly increased after NTG administration (12.3±3.0 vs. 17.1±4.6 mm^2, $P< 0.001$). V_E was significantly decreased after NTG administration (0.81±0.16 vs. 0.65±0.11 mmHg/%, $P < 0.001$). Percentage change of eA (%eA) was 39.6±18.2 % and percentage change of V_E (%V_E) was -19.5±10.4 %.

However, there was no significant correlation between the percentage change of brachial artery diameter by ultrasound and the percentage eA or percentage V_E (%eA: $r = 0.31$, $P = 0.25$, %V_E:$r = 0.19$, $P=0.48$).

Age-related vascular function: Baseline characteristics

In this additional analysis, we excluded 2 smokers because smoking attenuated vascular function. Thus, we analyzed a total of 14 subjects in this analysis.

There were 8 younger subjects (<35 years old)[45] (younger group) and 6 older subjects (older group). The baseline characteristics of the 2 groups are addressed in Table 1b. As expected, the older group was older than the younger group ($P< 0.001$). Otherwise, there were no significant differences between the 2 groups in terms of baseline characteristics.

Table 1b. Baseline characteristics of younger and older group

	Younger (n = 8)	Older (n = 6)	P-value
Age (years)	23.0±1.2	44.3±5.8	<0.001
Height (cm)	169.4±4.1	169.3±5.8	0.99
Weight (kg)	66.6±9.6	68.5±10.3	0.72
BMI (kg/m^2)	23.3±3.5	23.9±5.8	0.73
Systolic BP (mmHg)	118.1±17.0	107.8±6.6	0.18
Diastolic BP (mm Hg)	72.3±10.6	68.7±9.1	0.52
HR (bpm)	66.2±10.6	56.7±7.5	0.09
T-CHO (mg/dl)	193.3±32.6	204.5±50.2	0.61
LDL-CHO (mg/dl)	109.6±16.2	129.5±53.7	0.33
FBS (mg/dl)	88.3±9.3	87.5±7.0	0.87
HbA1c (%)	4.9±0.2	5.0±0.2	0.23

BMI; body mass index (kg/m^2),BP; blood pressure (mmHg),HR; heart rate (bpm), ;T-CHO; total cholesterol (mg/dl),LDL-CHO; low-density lipoprotein cholesterol (mg/dl)FBS; fasting blood sugar (mg/dl); HbA1c, haemoglobin A1c (%)

Association between eA, V_E and aging.

There was no significant difference in the rest ultrasound measurements of brachial artery diameter between the two groups (Younger: 3.79±0.38 vs. Older: 4.05±0.62, P = 0.35). Oscillometric measurement also did not show significant differences in rest eA between the two groups (Younger: 10.9±2.0 vs. Older: 13.3±3.8 mm^2, P= 0.15). In contrast, the older group showed significantly higher V_E compared to the younger group (Younger: 0.72±0.09 vs. Older: 0.95±0.14, P= 0.003).

There was no significant correlation between ultrasound-measured brachial artery diameter and age (r = 0.32, P = 0.26, Fig. 4a). In contrast, there was a significant correlation between eA and increasing age (r = 0.56, P = 0.026, Fig. 4b). Rest V_E also showed significant correlation with increasing age (r = 0.81, P< 0.001, Fig. 4c).

Fig. 4

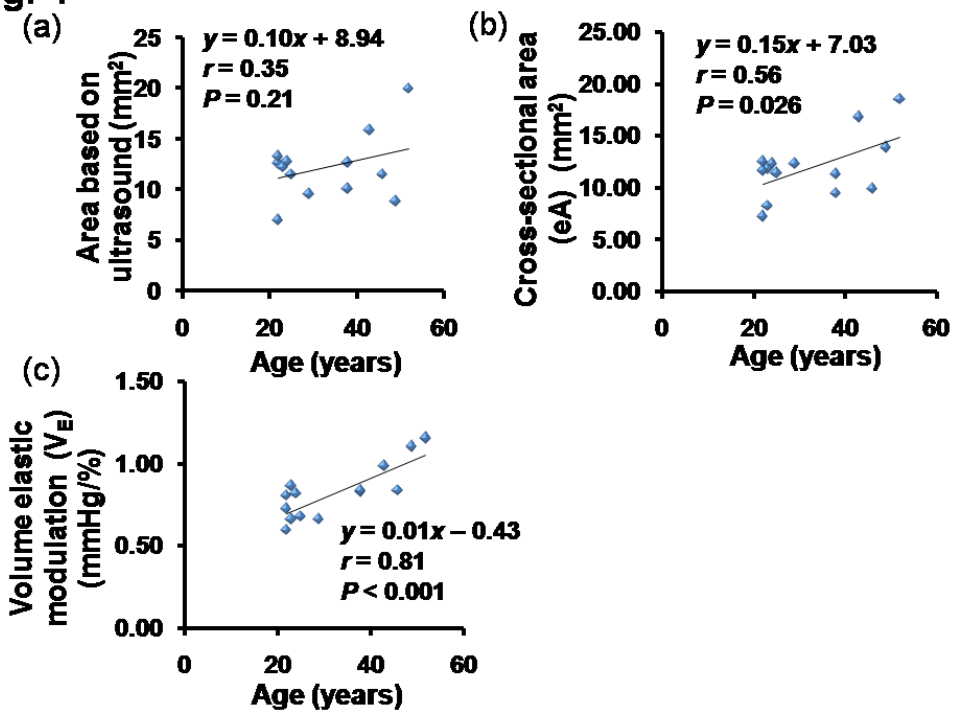

Fig. 4 Correlation between age and other parameters.

(a) Correlation between age and ultrasound measurements of brachial artery diameter.

(b) Correlation between age and oscillometric measurement of estimated cross-sectional area (eA).

(c) Correlation between age and oscillometric measurement of volume elastic modulus (V_E).

Discussion

The absolute value of rest brachial artery estimated cross-sectional area using oscillometric measurement showed good correlation with brachial artery ultrasound measurements. The estimated cross-sectional area and V_E measurements using this new modality showed good reproducibility. Oscillometric measurement automatically detected the changes in eA and V_E after NTG administration. In addition, eA and V_E increased in association with increasing age.

Reliability of automated oscillometric measurement: Comparison between oscillometric measurement and ultrasound measurements.

In the current system, the oscillometric method quantitatively estimates cross-sectional vascular area. In this study, we converted cross-sectional area to brachial vascular diameter in order to compare it with ultrasound measurements. The converted estimated arterial diameter was similar to that determined using ultrasound measurements. The rest estimated vascular diameter also significantly correlated with the ultrasound-measured brachial artery diameter. Therefore, this oscillometric method should be a reliable approach and may provide similar useful anatomical information to that determined by ultrasound measurement.

Ultrasound measurement provides a visualization of the vascular lumen and therefore allows for an exact measurement of the vascular diameter, whereas oscillometric methods do not provide for such visualization and therefore provide an approximation of the vascular cross-sectional area. Given the characteristics of the oscillometric approach, soft tissues surrounding arteries may be included in cross-sectional area measurements, possibly leading to an overestimation of volume. Even when this concern was taken into account, the current data showed good correlation with ultrasound measurements that are part of the standard approach[41]. In fact, the current data showed the estimated brachial vascular diameter to be slightly larger than brachial artery diameter determined using ultrasound. However, there was no significant difference between the two measurements.

The cross-sectional area estimation showed high ICC. Previous data reported that reproducibility of ultrasound brachial artery diameter measurement had an ICC of 0.84[53]. Oscillometric measurements agree with those of previous studies. Based on these data, oscillometric measurements would be reliable and can be used in clinical or epidemiological settings.

NTG response is an endothelium-independent vascular dilatation function[54]. In this study, eA significantly increased after NTG administration. The response to NTG was similar to that found using ultrasound. On the other hand, there was no correlation between the percentage change in diameter as measured by ultrasound and eA. The range of data for %NTG was narrow because of the normal study population. This may be a reason for the lack of correlation in NTG response between the two tests. Oscillometric measurements may have included brachial artery and surrounding vascular areas, and therefore the value of eA may have appeared to be higher than it was

found to be with ultrasound, especially under NTG stress. This also may have been the reason there was no significant correlation between percentage eA change with NTG stress determined by oscillometric measurement and that determined by ultrasound measurement. Although we did not show the correlation, the oscillometric approach was able to detect vascular cross-sectional area change during NTG stress.

Automated measurements of V_E

The rest V_E showed good reproducibility. This reproducibility is similar to that for other vascular functional evaluations[55].

Arterial elastic mechanics including $V_E$are linked to arterial stiffness[37, 38]. Bank et al reported that brachial artery elastic mechanics accurately evaluated vascular stiffness over a wide range of BP and vascular smooth muscle tone[40]. Therefore, V_E should be examined in clinical practice. However, previous methods of doing so were either complex or invasive[40, 41]. The current oscillometic approach may build on these previous studies and may allow for practical measurements of vascular elasticity in clinical settings or epidemiological study settings.

V_E was also reduced under NTG stress. NTG dilates brachial arteries by causing smooth muscle relaxation. The oscillometric system automatically detected changing vascular tone with NTG, and these data agree with those from the previous study by Bank et al[40]. The current data may imply that this approach could be used to detect anatomical and functional change during NTG stress.

Relation between eA, V_E and aging

In addition to showing the reliability of this new approach, we further looked at the association between those markers and age-related vascular anatomical and functional changes. Vascular function alters in association with aging[48, 51]. A previous study showed brachial artery diameter increases in relation to aging[31]. In this study, the older group tended to have higher brachial vascular diameter and eA. However, the differences between the values for the younger group and those for the older group were not significant, perhaps due to the small sample size with a wider range of standard deviation. Thus, our results may partly agree with those of previous studies. Further studies are required to confirm these data in a larger study population. On the other hand, over the total study population, rest eA showed significant correlation with increasing age. These data agree with previous data acquired using the same method[43].

Vascular stiffness and vascular function also alter in association with aging[51]. Rahmani-Cherati et al[56] reported that vascular elastisty was associated with vascular stiffness. Thus, attenuated V_E in the current study may indicate that older subjects had increasing vascular stiffness. The current data may agree with those of the previous study.

A previous study by Otsuka et al[43] showed very limited relationships between V_E and other cardiovascular risk factors including age, possibly due in part to the difference in the study design. In the previous study, subjects had BP measurements prior to oscillometric measurements and they did not have enough resting time before vascular function measurements[43]. These factors may have had a significant impact on vascular function such as V_E[41]. Further evaluation looking at the value of V_E measurements is required. In this study, we applied a standard approach to vascular function measurement[41, 57]. With the appropriate preparation, we showed that there were significant differences between the V_E measurements of the two groups. Moreover, increasing V_E was significantly correlated with increasing age. Other imaging methods such as ultrasound, positron emission tomography, and pulse wave velocity showed attenuated vascular function in the older population[51, 58, 59]. The current data agree with those from these previous studies. The current data add new insights regarding V_E to those from the previous study by Otsuka et al. This new method may be able to automatically detect age-related vascular dysfunction.

The current data show an association between rest eA and V_E with increasing age. Measuring brachial artery diameter and vascular elasticity might be useful in clinical and epidemiological settings for evaluating atherosclerosis.

Applied measurements model

In the present study, we measured V_E and eA while the vessel remained circular. We applied models for thin-walled tubes[42]. The current study population comprised healthy individuals whose arterial walls should be thin. Therefore, the current approach using thin-walled tube law should be appropriate.

When the vessel is compressed and buckles, measuring vascular area and diameter may become challenging. Therefore, we applied the measurement point before changing the vascular shape. However, the vessel may be buckled during measurement and so it would be important to develop a new algorithm to estimate the cross-sectional area of the buckled vessel. This should be the next step in the development of this oscillometric

measurement.

Some of the targeted study population who require vascular function measurements may have thick arterial walls. Therefore, it would be useful to add corrections factors to the thin-shelled theories[60] or to apply one-dimensional general tube law as proposed by Kozlovsky et al[61].

Limitations

Our study had a small population. The current protocol included two oscillometric measurements and one ultrasound study, each on a separate day (Figure 1). Since each study had rest and NTG stress, it would be difficult to apply this comprehensive study protocol to a large number of subjects. Even with a small sample size, with careful preparation we showed good reproducibility of eA and V_E.While a small sample size may have had a minimal impact on the current data, we definitely need further study using a larger study population and a simplified protocol.

All study subjects were male. Women have vascular functional changes during their menstrual cycle, which may have impacts on vascular function. For this initial study, we wanted to avoid these effects. However, we need to apply this measurement to women. Such studies are currently underway.

In the present study, we evaluated only normal individuals and smokers. Applying the current comprehensive protocol to CAD patients would have been difficult. However, this measurement technique should be applied to subjects with atherosclerotic risk factors and CAD patients as a next step.

In the present study, we applied the same pulse pressure, 40 mmHg, to estimate V_E. However, using individual pulse pressure would be ideal for setting P1. This possibility should be tested in the future and should be applied to this oscillometric measurement.

Conclusion

This new quantitative automated oscillometric measurement accurately assessed brachial artery cross-sectional area and vascular elasticity. This measurement technique can also detect morphological and functional change under NTG stress and is a reliable approach. Therefore, this modality may have practical application in quantitatively assessing muscular artery elasticity and diameter responses.

Conclusions

The quantification of myocardial blood flow (MBF) and coronary flow reserve (CFR) is a useful method for evaluating functional severity of the coronary artery disease, even in patients with balanced multivessel diseases and microcirculatory disturbances.

Arterial diameter enlargement is expected to be an early indicator in the progression of atherosclerosis. Enlargement of brachial artery diameter is related to the conventional cardiovascular risk factors.

In the first study, we compared MBF quantified from MRI with ^{15}O-H_2O PET, which yields standard MBF. We developed and validated the single-tissue compartment model to estimate MBF using dynamic perfusion MRI. MBF and CFR from MRI showed high reproducibility and a strong correlation with those from PET in the healthy subjects and our method using MRI yielded lower CFR in patients with coronary artery disease compared with the healthy subjects. This method is expected to demonstrate a wide range of applications in various patient populations.

In the second study, we compared diameter and elasticity of the brachial artery estimated from automated oscillometric measurement with ultrasound imaging. This new quantitative method accurately assessed brachial artery cross-sectional area and vascular elasticity. In addition, it can also detect morphological and functional change under nitroglycerin stress and is a reliable approach. Therefore, automated oscillometric measurement may have practical application in quantitatively assessing muscular artery elasticity and diameter responses.

In conclusion, we developed new methods which enable to detect coronary artery disease using MRI and early stage of atherosclerosis using automated oscillometric measurement. These methods enable to perform without special equipment or specially trained operator and to be widely used in clinical settings.

謝辞

本研究を進めていく上で多大な御指導、御鞭撻を賜りました、指導教官である北海道大学大学院医学研究科病態情報学講座核医学分野 玉木長良教授に心より厚く感謝の意を表します。玉木教授には臨床研究の経験の無い筆者を暖かく見守って頂き、研究に向かう姿勢や論文執筆に向けての研究方針を示して頂き深く感謝を申し上げます。

そして、学部在籍時より様々な御助言と激励を賜り、画像解析プログラミングを一から指導して頂いた北海道大学大学院保健科学院 加藤千恵次教授には厚くお礼を申し上げます。加藤教授には具体的な解析方法の提案や研究を進めやすい環境を整えて頂いたことに心より感謝を申し上げます。

加えて、臨床研究の実施及び本論文の作成に当たりご指導頂き、辛抱強く見守って下さいました北海道大学大学院医学研究科病態情報学講座核医学分野 真鍋治先生、放射線医学総合研究所分子イメージング研究センター 吉永恵一郎先生には深く感謝を申し上げます。また、研究用の検査の実施や英語論文の作成に関し御指導を賜りました、北海道大学病院放射線診断科 真鍋徳子先生、循環器内科 納谷昌直先生には重ねてお礼申し上げます。

画像検査におきましては、撮影に携わて頂いた北海道大学病院診療支援部放射線部 孫田恵一技師、杉森博之技師、堀江達之技師、北海道大学病院診療支援部放射線部 検査輸血部 西田睦技師、井上真美子技師、越智典樹技師に厚くお礼申し上げます。

大学院生活では、核医学分野秘書 鈴木江り子様、中村真樹子様、青山翼様、堀靖子様に大変お世話になりました。秘書の皆様のおかげで博士課程卒業まで学生生活を快適に送ることが出来ましたことに感謝申し上げます。

最後になりますが、本研究の遂行にあたってご協力を賜りました北海道大学大学院医学研究科の諸先生方、並びに、論文作成が進まず落ち込みがちな筆者を支えてくれた保健科学院の後輩、友人の皆様、両親、弟達、心から感謝をしたいと思います。皆様本当に有難うございました。

参考文献

1. White C. W.*, et al.* Does visual interpretation of the coronary arteriogram predict the physiologic importance of a coronary stenosis? *N Engl J Med* 310, 819-824 (1984).
2. Naya M. & Di Carli M. F. Myocardial perfusion pet/ct to evaluate known and suspected coronary artery disease. *J Nucl Med Mol Imaging* 54, 145-156 (2010).
3. Naya M.*, et al.* Quantitative relationship between the extent and morphology of coronary atherosclerotic plaque and downstream myocardial perfusion. *J Am Coll Cardiol* 58, 1807-1816 (2011).
4. Goldstein R. A.*, et al.* Relation between geometric dimensions of coronary artery stenoses and myocardial perfusion reserve in man. *J Clin Invest* 79, 1473-1478 (1987).
5. Yoshinaga K.*, et al.* Reduction of coronary flow reserve in areas with and without ischemia on stress perfusion imaging in patients with coronary artery disease: A study using oxygen 15-labeled water pet. *J Nucl Cardiol* 10, 275-283 (2003).
6. Tsukamoto T.*, et al.* Myocardial flow reserve is influenced by both coronary artery stenosis severity and coronary risk factors in patients with suspected coronary artery disease. *Eur J Nucl Med Mol Imaging* 33, 1150-1156 (2006).
7. Katoh C.*, et al.* Quantification of regional myocardial blood flow estimation with three-dimensional dynamic rubidium-82 pet and modified spillover correction model. *J Nucl Cardiol* 19, 763-774 (2012).
8. Kikuchi Y.*, et al.* Quantification of myocardial blood flow using dynamic 320-row multi-detector ct as compared with (1)(5)o-h(2)o pet. *European radiology* 24, 1547-1556 (2014).
9. Schwitter J.*, et al.* Assessment of myocardial perfusion in coronary artery disease by magnetic resonance: A comparison with positron emission tomography and coronary angiography. *Circulation* 103, 2230-2235 (2001).
10. Cheng A. S.*, et al.* Cardiovascular magnetic resonance perfusion imaging at 3-tesla for the detection of coronary artery disease: A comparison with 1.5-tesla. *J Am Coll Cardiol* 49, 2440-2449 (2007).
11. Jerosch-Herold M. & Kwong R. Y. Optimal imaging strategies to assess coronary blood flow and risk for patients with coronary artery disease. *Curr Opin Cardiol* 23, 599-606 (2008).
12. Parkka J. P.*, et al.* Comparison of mri and positron emission tomography for measuring myocardial perfusion reserve in healthy humans. *Magn Reson Med* 55, 772-779 (2006).
13. Morton G.*, et al.* Quantification of absolute myocardial perfusion in patients with

coronary artery disease: Comparison between cardiovascular magnetic resonance and positron emission tomography. *J Am Coll Cardiol* 60, 1546-1555 (2012).
14. Fritz-Hansen T.*, et al.* Quantification of mri measured myocardial perfusion reserve in healthy humans: A comparison with positron emission tomography. *J Magn Reson Imaging* 27, 818-824 (2008).
15. Ichihara T.*, et al.* Quantitative analysis of first-pass contrast-enhanced myocardial perfusion mri using a patlak plot method and blood saturation correction. *Magn Reson Med* 62, 373-383 (2009).
16. Morita K.*, et al.* Smoking cessation normalizes coronary endothelial vasomotor response assessed with 15o-water and pet in healthy young smokers. *J Nucl Med* 47, 1914-1920 (2006).
17. Furuyama H.*, et al.* Assessment of coronary function in children with a history of kawasaki disease using (15)o-water positron emission tomography. *Circulation* 105, 2878-2884 (2002).
18. Katoh C.*, et al.* Improvement of algorithm for quantification of regional myocardial blood flow using 15o-water with pet. *J Nucl Med* 45, 1908-1916 (2004).
19. Manabe O.*, et al.* Repeatability of rest and hyperemic myocardial blood flow measurements with 82rb dynamic pet. *J Nucl Med* 50, 68-71 (2009).
20. Mueller A.*, et al.* Dual-source radiofrequency transmission with patient-adaptive local radiofrequency shimming for 3.0-t cardiac mr imaging: Initial experience. *Radiology* 263, 77-85 (2012).
21. Sasaki M., Shibata E., Kanbara Y. & Ehara S. Enhancement effects and relaxivities of gadolinium-dtpa at 1.5 versus 3 tesla: A phantom study. *Magn Reson Med Sci* 4, 145-149 (2005).
22. Wong K.*, et al.* Image registration in myocardial perfusion mri. *Conf Proc IEEE Eng Med Biol Soc* 1, 453-454 (2005).
23. Klein R., Beanlands R. S. & deKemp R. A. Quantification of myocardial blood flow and flow reserve: Technical aspects. *J Nucl Cardiol* 17, 555-570 (2010).
24. Herrero P., Markham J., Shelton M. E. & Bergmann S. R. Implementation and evaluation of a two-compartment model for quantification of myocardial perfusion with rubidium-82 and positron emission tomography. *Circ Res* 70, 496-507 (1992).
25. Ishida M.*, et al.* Quantification of myocardial blood flow using model based analysis of first-pass perfusion mri: Extraction fraction of gd-dtpa varies with myocardial blood flow in human myocardium. *Magn Reson Med* 66, 1391-1399 (2011).
26. So A. & Lee T. Y. Quantitative myocardial ct perfusion: A pictorial review and the

current state of technology development. *J Cardiovasc Comput Tomogr* 5, 467-481 (2011).
27. Hsu L. Y.*, et al.* Quantitative myocardial perfusion analysis with a dual-bolus contrast-enhanced first-pass mri technique in humans. *J Magn Reson Imaging* 23, 315-322 (2006).
28. George R. T.*, et al.* Quantification of myocardial perfusion using dynamic 64-detector computed tomography. *Invest Radiol* 42, 815-822 (2007).
29. Furuyama H.*, et al.* Altered myocardial flow reserve and endothelial function late after kawasaki disease. *J Pediatr* 142, 149-154 (2003).
30. Reichenbach J. R.*, et al.* 1h t1 and t2 measurements of the mr imaging contrast agents gd-dtpa and gd-dtpa bma at 1.5t. *European radiology* 7, 264-274 (1997).
31. Green D. J.*, et al.* Impact of age, sex and exercise on brachial and popliteal artery remodelling in humans. *Atherosclerosis* 210, 525-530 (2010).
32. Glagov S.*, et al.* Compensatory enlargement of human atherosclerotic coronary arteries. *N Engl J Med* 316, 1371-1375 (1987).
33. Holewijn S.*, et al.* Brachial artery diameter is related to cardiovascular risk factors and intima-media thickness. *Eur J clin Inv* 39, 554-560 (2009).
34. Hamburg N. M.*, et al.* Cross-sectional relations of digital vascular function to cardiovascular risk factors in the framingham heart study. *Circulation* 117, 2467-2474 (2008).
35. Yoshinaga K., Manabe O. & Tamaki N. Assessment of coronary endothelial function using pet. *J Nucl Cardiol* 18, 486-500 (2011).
36. Wohlfahrt P.*, et al.* Lower-extremity arterial stiffness vs. Aortic stiffness in the general population. *Hypertens Res* 36, 718-724 (2013).
37. Kaiser D. R., Mullen K. & Bank A. J. Brachial artery elastic mechanics in patients with heart failure. *Hypertension* 38, 1440-1445 (2001).
38. O'Rourke M. F.*, et al.* Clinical applications of arterial stiffness; definitions and reference values. *American journal of hypertension* 15, 426-444 (2002).
39. Clairotte C.*, et al.* Automated ankle-brachial pressure index measurement by clinical staff for peripheral arterial disease diagnosis in nondiabetic and diabetic patients. *Diabetes care* 32, 1231-1236 (2009).
40. Bank A. J.*, et al.* Contribution of collagen, elastin, and smooth muscle to in vivo human brachial artery wall stress and elastic modulus. *Circulation* 94, 3263-3270 (1996).
41. Corretti M. C.*, et al.* Guidelines for the ultrasound assessment of endothelial-dependent flow-mediated vasodilation of the brachial artery: A report of the international brachial artery reactivity task force. *J Am Coll Cardiol* 39, 257-265 (2002).

42. Whittaker R. J., Heil M., Jensen O. E. & Waters S. L. A rational derivation of a tube law from shell theory. *Q J Mech Appl Math* 63, 465-496 (2010).
43. Otsuka T.*, et al.* Oscillometric measurement of brachial artery cross-sectional area and its relationship with cardiovascular risk factors and arterial stiffness in a middle-aged male population. *Hypertens Res* 36, 910-915 (2013).
44. Diamond G. A. & Forrester J. S. Analysis of probability as an aid in the clinical diagnosis of coronary-artery disease. *N Engl J Med* 300, 1350-1358 (1979).
45. Zimmerman F. H., Cameron A., Fisher L. D. & Ng G. Myocardial infarction in young adults: Angiographic characterization, risk factors and prognosis (coronary artery surgery study registry). *J Am Coll Cardiol* 26, 654-661 (1995).
46. Fukui M.*, et al.* Could home arterial stiffness index be a novel marker for arterial stiffness in patients with type 2 diabetes? *Hypertens Res* 36, 645-649 (2013).
47. Hu H.*, et al.* A cutoff point for arterial stiffness using the cardio-ankle vascular index based on carotid arteriosclerosis. *Hypertens Res* 36, 334-341 (2013).
48. Doonan R. J.*, et al.* Differences in arterial stiffness at rest and after acute exercise between young men and women. *Hypertens Res* 36, 226-231 (2013).
49. Hamburg N. M.*, et al.* Relation of brachial and digital measures of vascular function in the community: The framingham heart study. *Hypertension* 57, 390-396 (2011).
50. Liu L.*, et al.* Influence of personal exposure to particulate air pollution on cardiovascular physiology and biomarkers of inflammation and oxidative stress in subjects with diabetes. *J Occup Environ Med* 49, 258-265 (2007).
51. Celermajer D. S.*, et al.* Aging is associated with endothelial dysfunction in healthy men years before the age-related decline in women. *J Am Coll Cardiol* 24, 471-476 (1994).
52. Cohen J. A power primar. *Psychol Bull* 112, 155-159 (1992).
53. Meirelles Cde M., Leite S. P., Montenegro C. A. & Gomes P. S. Reliability of brachial artery flow-mediated dilatation measurement using ultrasound. *Arquivos brasileiros de cardiologia* 89, 160-167, 176-183 (2007).
54. Celermajer D. S.*, et al.* Passive smoking and impaired endothelium-dependent arterial dilatation in healthy young adults. *N Engl J Med* 334, 150-154 (1996).
55. Kinlay S.*, et al.* Endothelium-derived nitric oxide regulates arterial elasticity in human arteries in vivo. *Hypertension* 38, 1049-1053 (2001).
56. Rahmani-Cherati T., Mokhtari-Dizaji M. & Gity M. Association between atherosclerosis in carotid artery and elastic modulus of brachial artery. *J Teh Univ Heart Ctr* 1, 15-19 (2006).
57. Weber M. A.*, et al.* Clinical practice guidelines for the management of

hypertension in the community a statement by the american society of hypertension and the international society of hypertension. *J hypertens* 32, 3-15 (2014).

58. Uren N. G.*, et al.* Effect of aging on myocardial perfusion reserve. *J Nucl Med* 36, 2032-2036 (1995).
59. Alghatrif M.*, et al.* Longitudinal trajectories of arterial stiffness and the role of blood pressure: The baltimore longitudinal study of aging. *Hypertension* 62, 934-941 (2013).
60. Marzo A., Luo X. Y. & Bertram C. D. Three-dimensional collapse and steady flow in thick-walled flexible tubes. *J Fluid Struct* 20, 817-835 (2005).
61. Kozlovsky P., Zaretsky U., Jaffa A. J. & Elad D. General tube law for collapsible thin and thick-wall tubes. *J Biomech* 47, 2378-2384 (2014).